ELSEVIER

Journal of Fluids and Structures 21 (2005) 243–255

JOURNAL OF FLUIDS AND STRUCTURES

www.elsevier.com/locate/jfs

Reduced-order modeling for linearized aeroelasticity of fixed wings in transonic flight

U. Iemma*, M. Gennaretti

Department of Mechanical & Industrial Engineering, University Roma Tre, Via della Vasca Navale 79, 00146 Rome, Italy

Received 4 August 2004; accepted 14 May 2005
Available online 19 September 2005

Abstract

This paper presents a methodology for the identification of a reduced-order model (ROM) for the perturbation aeroelastic analysis of fixed wings in transonic flight. It is based on a linearized, frequency-domain, boundary-field integral equation for the solution of the unsteady perturbation potential flow about steady-state reference wing configurations. The resulting transfer functions between structural Lagrangean variables and generalized aerodynamic forces are approximated by means of rational expressions, and the aeroelastic ROM is identified by coupling them with the structural operator. With the aeroelastic operator recast in a reduced-order form, transonic flutter boundaries are detected through a classical eigenvalue analysis and the time-domain state–space aeroelastic model is also obtained. Applications of the methodology presented to a widely known aeroelastic test case reveal a remarkable agreement with the measured speed and frequency of flutter.

Keywords: Wing aeroelasticity; Reduced-order models; Transonic flows

1. Introduction

A reduced-order model (ROM) for the unsteady aerodynamics of flexible wings in the transonic regime is presented and coupled with the structural operator yielding a ROM for the complete aeroelastic operator. Because of the highly time-consuming, time-marching nonlinear approaches typically applied to the aeroelastic analysis of fixed wings in transonic flows, the availability of an aeroelastic model based on an aerodynamic ROM would be extremely convenient. This is particularly true in flutter detection, where it allows the identification of the stability boundaries through classical eigenproblem analysis, without the need of introducing iterative methods such as p–k or V–g. In addition, in the time domain, the availability of an aerodynamic ROM is the essential condition for recasting the aeroelastic problem in state–space format. The state–space format is particularly attractive for control purposes and preliminary design analysis, where accurate but simple mathematical models are desired. Several different techniques have been developed in the last decade to extract reduced-order models of nonlinear systems. One of the most widely used in aeroelastic modeling is based on the application of the Volterra theory on the impulse response provided by unsteady CFD solvers [see, e.g., Silva and Bartels (2004)]. An extensive review of the most recent research on reduced-order modeling is given in Lucia et al. (2004).

*Corresponding author. Tel.: +39 06 55173274; fax: +39 06 5593732.
E-mail address: u.iemma@uniroma3.it (U. Iemma).

0889-9746/$ - see front matter © 2005 Elsevier Ltd. All rights reserved.
doi:10.1016/j.jfluidstructs.2005.05.014

In the present paper, it is assumed that the unsteady transonic flow can be approximated by the superposition of a nonlinear mean steady flow with a linear unsteady small perturbation flow. Similar approaches have been examined in the past by Fung et al. (1978), Williams (1979) and Ehlers and Weatherill (1982). The unsteady perturbation velocity field is solved in the frequency domain by a linearized boundary-field integral equation for the unknown potential. The aerodynamic transfer functions between wing structural Lagrangean variables and aerodynamic generalized forces are derived by the application of Bernoulli's theorem followed by projection of pressure loads onto the shape functions chosen for the description of wing elastic deformation. These generalized aerodynamic forces are approximated by finite-pole rational expressions that, coupled with the structural dynamics operator, allow the identification of flutter stability boundaries by a classical eigenvalue analysis. In addition, transforming the problem into the time domain, gives the aeroelastic ROM in a state–space format that involves the structural Lagrangean variables and some additional aerodynamic states. The additional aerodynamic states arise because of the presence of a finite number of poles in the rational aerodynamic transfer functions. In turn, these poles are introduced for approximating the effects of the transcendental terms appearing in the original aerodynamic transfer functions due to the unsteady vorticity convected along the wake and the finite value of the speed of sound in compressible flows (Gennaretti and Mastroddi, 2004).

A numerical investigation concerning the analysis of the effects of flow compressibility on the aerodynamic transfer functions, and the detection of flutter boundaries in transonic flow regimes for a widely used test case available in the literature will be presented.

2. Integral equation for linearized transonic aerodynamics

The isentropic irrotational flow of a compressible inviscid fluid is described by the full-potential model. The advantage of using the velocity potential function, ϕ, such that $\vec{v} = \nabla\phi$, resides in the reduction of the problem to the evaluation of a single scalar field, with the limitation that entropy variations and vorticity cannot be predicted. It has been widely demonstrated that these limitations are acceptable for the evaluation of the unsteady aerodynamic loads if the vibrations of airplane wings at cruising conditions are constrained to small amplitudes and, in addition, the airfoil thickness is assumed to be small. Indeed, in such a flow the vorticity is confined in a narrow region and the shock waves are usually weak. For these reasons, the full-potential model is still of primary interest for aeroelastic applications. By combining the continuity equation with Bernoulli's theorem for isentropic potential compressible flows, and taking into account the isentropic density–enthalpy relationship (Iemma and Morino, 1997), the full-potential equation reads

$$\nabla^2\phi - \frac{1}{c_\infty^2}\frac{\partial^2\phi}{\partial t^2} = \sigma, \tag{1}$$

where c_∞ is the undisturbed flow speed of sound and σ represents the nonlinear terms. The expression for σ depends on the form of the continuity equation used for the derivation of Eq. (1) (Iemma and Morino, 1997). The flow is assumed to be bounded by the surface $\mathsf{S} = \mathsf{S}^B \cup \mathsf{S}^W$, where S^B and S^W are wing and wake surfaces, respectively. Denoting by V the flow region where the nonlinear terms are not negligible and for unperturbed flow condition at infinite distance from the wing, the boundary integral formulation, in a wing-fixed frame of reference, yields the following transonic flow potential solution (Iemma and Morino, 1997):

$$\phi(\vec{x},t) = \int_{\mathsf{S}} \left[G\frac{\partial\phi}{\partial\hat{n}} - \phi\frac{\partial G}{\partial\hat{n}} + \dot{\phi}\, G\frac{\partial\hat{\theta}}{\partial\hat{n}} \right]^{\theta} \mathrm{d}\mathsf{S}(\vec{y}) + \int_{\mathsf{V}} G[\sigma]^{\theta}\,\mathrm{d}\mathsf{V}(\vec{y}). \tag{2}$$

In this equation,

$$G(\vec{x},\vec{y}) = \frac{-1}{4\pi r_\beta}$$

is the space distribution of the unit source solution of Eq. (1), and $r_\beta = \{[\vec{m}_B\cdot(\vec{y}-\vec{x})]^2 + \beta^2\|\vec{y}-\vec{x}\|^2\}^{1/2}$, with $\vec{m}_B = \vec{v}_B/c_\infty$ denoting the Mach vector of the wing velocity, $\vec{v}_B$, and $\beta = \sqrt{1-m_B^2}$. In addition, $[]^\theta$ indicates evaluation at the retarded time $t-\theta$, where $\theta = [r_\beta - \vec{m}_B\cdot(\vec{y}-\vec{x})]/c_\infty\beta^2$ is the time required by a perturbation to travel from $\vec{y}$ to $\vec{x}$ (acoustic time delay), $\hat{\theta} = [r_\beta + \vec{m}_B\cdot(\vec{y}-\vec{x})]/c_\infty\beta^2$, whereas $\vec{n}$ denotes the wing outward unit

normal, and

$$\frac{\partial(\cdot)}{\partial\hat{n}} = \frac{\partial(\cdot)}{\partial n} - \vec{m}_B \cdot \vec{n}\, \vec{m}_B \cdot \vec{\nabla}(\cdot).$$

Within the present scope, i.e., the identification of a transonic aeroelastic ROM via linearization of the aerodynamic operator, the use of the following nonconservative form of σ is convenient (it depends on integer powers of ϕ and $\nabla\phi$):

$$\sigma = (c_\infty^2 - c^2)\frac{\nabla^2\phi}{c_\infty^2} + \frac{2\,\vec{v}\cdot\partial\vec{v}/\partial t}{c_\infty^2} + \frac{\vec{v}}{2c_\infty^2}\cdot\nabla v^2. \tag{3}$$

Since the natural application of linearized operators deals with small perturbations around a reference configuration, the use of the nonconservative form for σ does not affect significantly the accuracy of the perturbation solution. However, this is not true when dealing with the steady reference field, for which the conservation form of the equation represents a crucial point since it guarantees the satisfaction of the mass conservation law even in the presence of strong shocks. See, for example the references by Jameson (1975) and, for integral formulations, Morino and Iemma (1993). Indeed, for the numerical evaluation of the steady reference aerodynamic solution the nonlinear terms, σ_0, are obtained through the conservative form, with the full-potential model completed by the application of the Bernoulli theorem for the determination of the local speed of sound (Iemma and Morino, 1997) that reads

$$\frac{c^2}{c_\infty^2} = 1 - \frac{\gamma-1}{c_\infty^2}\left(\frac{\partial\phi}{\partial t} + \frac{v^2}{2}\right).$$

As mentioned above, the basic issue in the reduced-order modeling presented in this paper is the definition of the frequency-domain linearized version of the boundary-field integral equation, Eq. (2). The unsteady potential is assumed to be given by the superposition of the steady reference solution, ϕ_0, with a small perturbation potential field, φ, so that $\phi = \phi_0 + \varphi$ and hence $\vec{v} = \nabla(\phi_0 + \varphi) = \vec{v}_0 + \vec{v}$, with $\vec{v}$ denoting the perturbation velocity field. Then, substituting into Eq. (3) and retaining only the terms depending linearly on φ, yields the following expression for the small perturbation component of the field contribution in Eq. (2):

$$\varsigma = A_1\nabla^2\varphi + A_2\dot{\varphi} + \vec{A}_3\cdot\vec{v} + \vec{A}_4\cdot\dot{\vec{v}} + \frac{\vec{A}_4}{2}\cdot\nabla(\vec{v}_0\cdot\vec{v}),$$

where the coefficients have the form

$$A_1 = \frac{\gamma-1}{c_\infty^2}\left(\vec{v}_B\cdot\vec{v}_0 + \frac{v_0^2}{2}\right),$$

$$A_2 = \frac{\gamma-1}{c_\infty^2}\nabla^2\phi_0,$$

$$\vec{A}_3 = \frac{1}{c_\infty^2}\left[(\gamma-1)\nabla^2\phi_0(\vec{v}_0 + \vec{v}_B) + \frac{1}{2}\nabla v_0^2\right],$$

$$\vec{A}_4 = \frac{2}{c_\infty^2}\vec{v}_0.$$

The final steps of the derivation are: (i) recasting the nonlinear terms in Eq. (2) as $\sigma = \sigma_0 + \varsigma$, (ii) elimination of the constant terms that satisfy the integral equation for ϕ_0 and (iii) transformation into the Laplace domain. These yield the following linear boundary-field integral equation for the perturbation potential:

$$\tilde{\varphi}(\vec{x}) = \int_{\mathsf{S}}\left(G\frac{\partial\tilde{\varphi}}{\partial\hat{n}} - \tilde{\varphi}\frac{\partial G}{\partial\hat{n}} + s\,\tilde{\varphi}\,G\,\frac{\partial\hat{\theta}}{\partial\hat{n}}\right)\mathrm{e}^{-s\theta}\,\mathrm{d}\mathsf{S}(\vec{y}) + \int_{\mathsf{V}} G\,\tilde{\varsigma}\,\mathrm{e}^{-s\theta}\,\mathrm{d}\mathsf{V}(\vec{y}), \tag{4}$$

where the tilde indicates Laplace transformation.

3. Linearized transonic BEM

In this section, Eq. (4) is discretized so as to get a version of it that is suitable for numerical applications. This is obtained through the a zeroth-order boundary-field element method (BEM): (i) wing and wake surfaces are divided into

M panels, S^B_m, and N panels, S^W_n, respectively; (ii) the field domain of interest, V, is divided into Q six face boundary volumes, V_q; (iii) potential, φ, and its derivatives are assumed to be constant over panels and volumes and equal to the values at mid-points (centroids), $\vec{y}_k$. Then, Eq. (4) evaluated at the centroids of the discretized configuration yields the following set of $N_t = M + Q$ algebraic equations for the perturbation potential:

$$H_k\,\tilde{\varphi}_k = \sum_{m=1}^{M}[B_{km}\,\tilde{\chi}_m + (C_{km} + sD_{km})\,\tilde{\varphi}_m] - \sum_{m=1}^{M}\vec{L}_{km}\cdot\nabla\tilde{\varphi}_m + \sum_{n=1}^{N}(F_{kn} + sG_{kn})\,\Delta\tilde{\varphi}_n + \sum_{q=1}^{Q}[sR_{kq}\,\tilde{\varphi}_q + (\vec{M}_{kq} + s\vec{P}_{kq})\cdot\nabla\tilde{\varphi}_q], \tag{5}$$

where $\varphi_m = \varphi(\vec{y}_m)$, $\chi_m = \vec{v}_B\cdot\vec{n}(\vec{y}_m)$, $\Delta\varphi_n$ is the potential jump across the nth wake panel, $\nabla\varphi_m = \nabla\varphi(\vec{y}_m)$, and $H_k = 1/2$ for $\vec{x}_k \in \mathsf{S}^B$ whereas $H_k = 1$ for $\vec{x}_k \in \mathsf{V}$. The coefficients in Eq. (5) are defined as

$$B_{km} = \mathrm{e}^{-s\,\theta_{km}}\int_{\mathsf{S}^B_m} G_k\,\mathrm{d}\mathsf{S},$$

$$C_{km} = \mathrm{e}^{-s\,\theta_{km}}\int_{\mathsf{S}^B_m}\frac{\partial G_k}{\partial\hat{n}}\,\mathrm{d}\mathsf{S},$$

$$D_{km} = \mathrm{e}^{-s\,\theta_{km}}\int_{\mathsf{S}^B_m} G_k\frac{\partial\hat{\theta}_k}{\partial\hat{n}}\,\mathrm{d}\mathsf{S},$$

$$\vec{L}_{km} = \left[A^m_1\vec{n}_m + \frac{\vec{A}^m_4\cdot\vec{n}_m}{2}\,\vec{v}^m_0\right]\mathrm{e}^{-s\,\theta_{km}}\int_{\mathsf{S}^B_m} G_k\,\mathrm{d}\mathsf{S},$$

$$R_{kq} = A^q_2\,\mathrm{e}^{-s\,\theta_{kq}}\int_{\mathsf{V}_q} G_k\,\mathrm{d}\mathsf{V},$$

$$\vec{P}_{kq} = \vec{A}^q_4\mathrm{e}^{-s\,\theta_{kq}}\int_{\mathsf{V}_q} G_k\,\mathrm{d}\mathsf{V},$$

$$\vec{M}_{kq} = \mathrm{e}^{-s\,\theta_{kq}}\left\{\vec{A}^q_3\int_{\mathsf{V}_q} G_k\,\mathrm{d}\mathsf{V} - \left[A^q_1\,\mathsf{I} + \frac{1}{2}\vec{v}^q_0\otimes\vec{A}^q_4\right]\sum_{j=1}^{6}\vec{n}_j\int_{\mathsf{S}^j_q} G_k\,\mathrm{d}\mathsf{S}\right\},$$

with I denoting the unit tensor, S^j_q denoting the jth face of V_q, and $\vec{v}^m_0$ and $\vec{n}_m$ denoting, respectively, the steady-state trim flow velocity and the outward unit normal at $\vec{y}_m$. Moreover, $G_k = G(\vec{y},\vec{x}=\vec{x}_k)$, $\hat{\theta}_k = \hat{\theta}(\vec{y},\vec{x}=\vec{x}_k)$, θ_{km} is the time taken by a signal emitted at $\vec{y}_m$ to reach $\vec{x}_k$, while F_{kn} and G_{kn} have the same expressions as C_{km} and D_{km}, respectively, with the integrals evaluated over the wake panels.

A convenient matrix form of Eq. (5) is obtained by expressing the vector quantities in terms of their components in a wing-fixed frame of reference and by recasting all contributions depending on the perturbation potential in terms of its values at the centroids (i.e., the unknowns of the algebraic equations). For $\vec{v}_j = \nabla\varphi_j$ and with $(\vec{i}_1,\vec{i}_2,\vec{i}_3)$ denoting the base vectors of the frame of reference, we introduce the $[3\times M]$ matrix $\mathbf{V}^B$ with the entries given by $V^B_{ij} = \vec{i}_i\cdot\vec{v}_j$, for $\vec{y}_j \in \mathsf{S}^B$ and the $[3\times Q]$ matrix $\mathbf{V}^F$ with the entries given by $V^F_{ij} = \vec{v}_j\cdot\vec{i}_i$, for $\vec{y}_j \in \mathsf{V}$. Then, using a finite-difference scheme for the discretization of the gradient operator, it is possible to define a $[3\times M\times N_t]$ gradient matrix $\mathbf{G}^B_{gr}$ and a $[3\times Q\times N_t]$ gradient matrix $\mathbf{G}^F_{gr}$ such that

$$\mathbf{V}^B = \mathbf{G}^B_{gr}\,\boldsymbol{\varphi} \quad\text{and}\quad \mathbf{V}^F = \mathbf{G}^F_{gr}\,\boldsymbol{\varphi},$$

with $\boldsymbol{\varphi}$ denoting the N_t-element column matrix that collects the (unknown) values of potential at the body centroids (the first M entries collected in the sub-column matrix $\boldsymbol{\varphi}^B$) and at the field centroids (the last Q entries collected in the sub-column matrix $\boldsymbol{\varphi}^F$). In addition, it is convenient to recast the wake contribution in terms of the potential unknowns. First, observe that [see, for instance, Morino and Iemma (1993)]

$$\Delta\varphi_n(t) = \Delta\varphi^{TE}_n(t-\tau_n),$$

where $\Delta\varphi^{TE}_n$ denotes the jump of potential at the wing trailing edge from which the nth wake panel was generated, whereas τ_n is the time taken by the wake point to move from the trailing edge to the nth wake panel. Thus, noting that in the frequency domain this yields

$$\Delta\tilde{\varphi}_n = \mathrm{e}^{-s\,\tau_n}\Delta\tilde{\varphi}^{TE}_n,$$

and introducing a matrix S_{nm} relating trailing-edge jumps of potential with potential at body centroids, we have

$$\Delta\tilde{\varphi}_n = \sum_{m=1}^{M} \mathrm{e}^{-s\,\tau_n} S_{nm}\tilde{\varphi}_m,$$

or, in matrix form,

$$\boldsymbol{\Delta}\tilde{\boldsymbol{\varphi}} = \mathbf{S}(s)\,\tilde{\boldsymbol{\varphi}}^{B},$$

with $\mathbf{S}$ of dimensions $[N \times M]$. For recasting the problem in matrix form, also vector coefficients $\vec{L}_{km}$, $\vec{P}_{kq}$ and $\vec{M}_{kq}$ have to be expressed in terms of their components in the wing frame. This is obtained by introducing the matrices $\mathbf{L}, \mathbf{M}, \mathbf{P}$ defined as follows:

$$L_{kmi} = \vec{L}_{km} \cdot \vec{i}_i \quad ([\mathbf{L}] = [N_t \times M \times 3]),$$
$$M_{kqi} = \vec{M}_{kq} \cdot \vec{i}_i \quad ([\mathbf{M}] = [N_t \times Q \times 3]),$$
$$P_{kqi} = \vec{P}_{kq} \cdot \vec{i}_i \quad ([\mathbf{P}] = [N_t \times Q \times 3]).$$

Furthermore, coefficients B_{km}, C_{km}, D_{km} are collected into matrices $\mathbf{B}, \mathbf{C}, \mathbf{D}$ of dimensions $[N_t \times M]$, coefficients F_{kn}, G_{kn} are collected into matrices $\mathbf{F}, \mathbf{G}$ of dimensions $[N_t \times N]$, coefficients R_{kq} are collected into the matrix $\mathbf{R}$ of dimensions $[N_t \times Q]$, and matrices $\mathbf{T}^B$ of dimensions $[M \times N_t]$ and $\mathbf{T}^F$ of dimensions $[Q \times N_t]$ are introduced to obtain the relationships $\boldsymbol{\varphi}^B = \mathbf{T}^B\,\boldsymbol{\varphi}$ and $\boldsymbol{\varphi}^F = \mathbf{T}^F\,\boldsymbol{\varphi}$. Finally, with the square matrix $\mathbf{T}$ of dimensions $[N_t \times N_t]$ defined as

$$\mathbf{T} = \begin{bmatrix} \frac{1}{2}\,\mathbf{T}^B \\ \mathbf{T}^F \end{bmatrix},$$

and with the M-element column matrix $\boldsymbol{\chi}$ collecting the boundary conditions, χ_m, Eq. (5) may be recast in matrix form and the linearized transonic perturbation-potential solution is given by

$$\tilde{\boldsymbol{\varphi}} = \mathbf{E}^{\varphi}_{tr}(s)\,\tilde{\boldsymbol{\chi}}, \tag{6}$$

with the following BEM solution matrix:

$$\mathbf{E}^{\varphi}_{tr}(s) = \{\mathbf{T} - [\,\mathbf{C} + s\,\mathbf{D} + (\mathbf{F} + s\,\mathbf{G})\,\mathbf{S}(s)\,]\mathbf{T}^B + \mathbf{L}\,\mathbf{G}^B_{gr} - s\,\mathbf{R}\,\mathbf{T}^F - (\mathbf{M} + s\,\mathbf{P})\,\mathbf{G}^F_{gr}\}^{-1}\mathbf{B}.$$

4. Transonic aeroelastic ROM

In this section, the aerodynamic matrix is described that, in a linear(ized) frequency-domain aerodynamic problem, relates the elastic displacements to the aerodynamic forces acting on the wing. Then, an aerodynamic ROM is derived that is extremely convenient for aeroelastic applications.

The derivation of the aerodynamic matrix has already been presented in the past for subsonic-flow analysis (Gennaretti and Ponzi, 1999; Gennaretti et al., 2000). Here, the novelty is that the aerodynamic matrix is derived for a transonic-flow problem and describes the forces arising from perturbations to a transonic steady-state equilibrium condition. Note that in the transonic regime, to each steady-state condition corresponds a specific transonic aerodynamic matrix, because of the dependence of the latter on the flight Mach number. The aerodynamic matrix is based on the linearized BEM perturbation solution described in the previous section and on the description of the wing elastic deformations through the following combination of N_v shape functions, $\vec{\Psi}_n$, and Lagrangean variables, q_n,

$$\vec{d}(\xi^1, \xi^2, t) = \sum_{n=1}^{N_v} q_n(t)\,\vec{\Psi}_n(\xi^1, \xi^2), \tag{7}$$

where (ξ^1, ξ^2) denotes a set of curvilinear coordinates defined over the surface of the wing. Indeed, following the procedure described in the Appendices A–C, in the frequency domain it is possible to define (i) a matrix $\mathbf{E}^{\chi}$ relating the Lagrangean variables, q_n, with the aerodynamic boundary conditions at the wing centroids, χ_m, [see Appendix A, Eq. (A.1)], (ii) a matrix $\mathbf{E}^{p}$ relating the potential values, φ_m, at the centroids with the perturbation pressure, p'_m, [see Appendix B, Eq. (B.1)] and (iii) a matrix $\mathbf{E}^{f}$ relating the latter with the generalized aerodynamic forces, f_n [see Appendix

C, Eq. (C.1)]. The combination of these matrices yields the following deformation/force relation:

$$\tilde{\mathbf{f}} = \mathbf{E}(s)\,\tilde{\mathbf{q}}, \tag{8}$$

where the aerodynamic matrix is given by

$$\mathbf{E}(s) = \mathbf{E}^{f}\,\mathbf{E}^{p}(s)\,\mathbf{E}^{\varphi}_{tr}(s)\,\mathbf{E}^{\chi}(s).$$

The aeroelastic model is obtained by coupling Eq. (8) with the wing structural model. Starting from the equations describing the wing dynamics, the aeroelastic model is determined by the Galërkin approach based on the shape function expansion in Eq. (7). Thus, for $\mathbf{M}_s$ and $\mathbf{K}_s$ denoting, respectively, structural mass and stiffness matrices, the frequency-domain aeroelastic model reads

$$\left[s^2\,\mathbf{M}_s + \mathbf{K}_s - \mathbf{E}(s)\right]\tilde{\mathbf{q}} = \mathbf{0}. \tag{9}$$

The time delays in disturbance propagation induced by flow compressibility and by the memory effects stored in the convected wake vorticity [respectively, θ_{km} and τ_n in Eq. (5)], cause a transcendental dependence on frequency of the aerodynamic matrix . In turn, this implies both that the aeroelastic stability analysis cannot be performed through a standard eigenanalysis (the associated eigenproblem has a transcendental characteristic equation with infinite roots), and that it is not possible to formulate the problem in a time-domain state–space format, unless an infinite-dimension state–space model is used. These difficulties are overcome by using the procedure introduced by Ghiringhelli and Mantegazza (1993) that approximates $\mathbf{E}(s)$ through the following second-order rational expression involving a finite number of poles

$$\mathbf{E}(s) \approx s^2\mathbf{A}_2 + s\mathbf{A}_1 + \mathbf{A}_0 + \mathbf{H}\left[s\,\mathbf{I} - \mathbf{A}_p\right]^{-1}\mathbf{Q}, \tag{10}$$

where $\mathbf{A}_2, \mathbf{A}_1, \mathbf{A}_0, \mathbf{A}, \mathbf{H}$ and $\mathbf{Q}$ are real, fully populated matrices obtained from a least-squares approach. Applications of this technique to the analysis of linear subsonic flows are presented in Gennaretti and Ponzi (1999) and Gennaretti et al. (2000) for wing-tail configurations and hovering rotors, respectively. Matrices $\mathbf{A}_2, \mathbf{A}_1$ and $\mathbf{A}_0$ have dimensions $[N_v \times N_v]$, $\mathbf{A}_p$ is a $[N_a \times N_a]$ matrix containing the N_a poles of the rational approximation, $\mathbf{H}$ is a $[N_v \times N_a]$ matrix, while $\mathbf{Q}$ has dimensions $[N_a \times N_v]$. Note that, in the expression above, the second-order polynomial truncation is suggested by the fact that the asymptotic behavior of transfer functions between elastic displacements and aerodynamic forces is quadratic, as induced by the presence of the first time derivative of the velocity potential in the Bernoulli theorem, together with the time derivative appearing in the aerodynamic boundary conditions (see matrices $\mathbf{E}^{p}$ and $\mathbf{E}^{\chi}$ in Appendices A and B).

Finally, the transonic-flow aeroelastic ROM is obtained by combining Eq. (10) with Eq. (9). This yields standard eigenproblems for flutter detection purposes whereas, in the time domain, it has the form of a state–space model that is well suited for control and other applications (e.g., preliminary design) that need accurate predictions at low computational costs. Specifically, in the time domain, the aeroelastic ROM is

$$\dot{\mathbf{x}} = \mathbf{A}\,\mathbf{x}$$

with

$$\mathbf{A} = \begin{bmatrix} \mathbf{0} & \mathbf{I} & \mathbf{0} \\ \breve{\mathbf{M}}^{-1}(\mathbf{A}_0 - \mathbf{K}_s) & \breve{\mathbf{M}}^{-1}\mathbf{A}_1 & \breve{\mathbf{M}}^{-1}\mathbf{H} \\ \mathbf{Q} & \mathbf{0} & \mathbf{A}_p \end{bmatrix},$$

where

$$\breve{\mathbf{M}} = (\mathbf{M}_s - \mathbf{A}_2)$$

and

$$\mathbf{x} = \begin{Bmatrix} \mathbf{q} \\ \dot{\mathbf{q}} \\ \mathbf{r} \end{Bmatrix},$$

with $\mathbf{r}$ denoting the additional states that have been included because of the presence of the aerodynamic poles in Eq. (10). Flutter boundaries are detected from the knowledge of the $2N_v + N_a$ eigenvalues of matrix $\mathbf{A}$.

5. Numerical results

The aeroelastic ROM presented above has been applied to the wing model analyzed by Guruswamy and Goorjian (1982). The wing model is a rectangular, untwisted wing with aspect ratio 5 and a circular biconvex section with thickness ratio 0.06. This simple model has been widely used in the past for validation of several aeroelastic transonic formulations. The availability of the experimental data from the wind-tunnel test conducted in the NASA Langley 16-ft transonic aeroelasticity wind tunnel and reported in Doggett et al. (1959), makes the study particularly appealing for the validation of numerical models. Following Guruswamy and Goorjian (1982), the flutter mechanism of the wing is described as the combination of first bending and torsion modes. These are approximated with the shape functions suggested by Fung (1969) that, for x denoting a chordwise coordinate, y denoting a spanwise coordinate, and l denoting the spanwise length, are given by

$$\Psi_b(x,y) = \left(\frac{y}{l}\right)^2, \quad \Psi_t(x,y) = x\left(\frac{y}{l}\right),$$

for bending and torsional out-of-midplane displacement, respectively.

As a first step, the influence of the flight Mach number, m_∞, on the aerodynamic transfer functions is investigated. The results of the parametric analysis are presented in Figs. 1–4, for the real and imaginary part of entries E_{11} and E_{12} of the aerodynamic matrix, $\mathbf{E}$ (in these figures, $M \equiv m_\infty$). The reduced frequency, k, is defined as $k = \omega c/v_\infty$, where c denotes the chord length. The Mach number is gradually increased from the incompressible limit up to $m_\infty = 0.9$. Fig. 5 depicts the local Mach number distribution at the wing root section, for five different flight speeds. As it can be seen, the flow becomes transonic about at $m_B = 0.85$, i.e., when the local flow speed reaches the speed of sound. For higher values of m_B, a shock wave is present in the flow. At $m_B = 0.9$, the maximum value of the local Mach number approaches 1.3, thus remaining in the range of applicability of the isentropic shock model. The extent of the supersonic region at this flight speed is shown in Fig. 6. The figure depicts the density plot of the local Mach number over the wing surface at $m_B = 0.9$. The local iso-mach line $m = 1$ (dotted line) shows that the flow is supersonic over a wide region of the wing surface.

The considerable impact of flight Mach number on the aerodynamic matrix is evident for all its elements. A careful examination of the results may give an insight into the physics of the phenomenon and on its impact on the ROM. Specifically, it is possible to identify four different regimes:

(i) for $m_\infty \leqslant 0.2$ the curves are almost identical, indicating that the effects of the flow compressibility are negligible in that range;
(ii) at $m_\infty = 0.4$, although the overall *shape* of the curves resembles that observed in the previous case, it is evident that the flow compressibility plays a significant role;
(iii) for $0.6 \leqslant m_\infty \leqslant 0.8$ the effects of the nonlinear terms in the reference steady-state solution (and of the corresponding linearized contribution to the aerodynamic matrix) is important, and significantly affect the frequency dependence of the aerodynamic transfer functions;
(iv) for $m_\infty \geqslant 0.85$ the steady flow is transonic (see Fig. 5), the linearized terms dominate the aerodynamic matrix, and the frequency behavior of its entries dramatically changes.

It clearly appears that, the larger the nonlinear transonic effects, the wavier the elements of $\mathbf{E}$ become as a function of the reduced frequency. As a consequence, the rational approximation of the aerodynamic matrix must include additional poles to properly reproduce this frequency dependance.

For the present problem, 19 poles have been used in the range $0 \leqslant k \leqslant 1$. The result of the approximation is presented in Figs. 7 and 8 for the transfer function relating the torsion moment to the bending displacement (element E_{21}). Figs. 7 and 8 depict the comparison between the frequency BEM solution and its rational approximation in terms of real and imaginary parts, respectively. The agreement is excellent and the same level of accuracy is shown by all of the remaining entries of the aerodynamic matrix.

The ROM obtained with the above approximation of $\mathbf{E}$ is used to predict the flutter boundaries for the test wing examined. These results, given in terms of nondimensional speeds and reduced frequencies of flutter, are presented in Tables 1 and 2 for the Mach numbers considered by Guruswamy and Goorjian (1982). Following Guruswamy and Goorjian (1982), the nondimensional speed is defined as $\hat{U} = 2v_\infty/c\omega_t$, with ω_t denoting wing natural frequency of torsion.

In Tables 1 and 2 the flutter speed and the flutter frequencies are compared with the experimental and numerical results given by Guruswamy and Goorjian (1982). For the three regimes analyzed, the agreement of the ROM numerical results with the experimental data is remarkable, and appears to be more accurate than the numerical

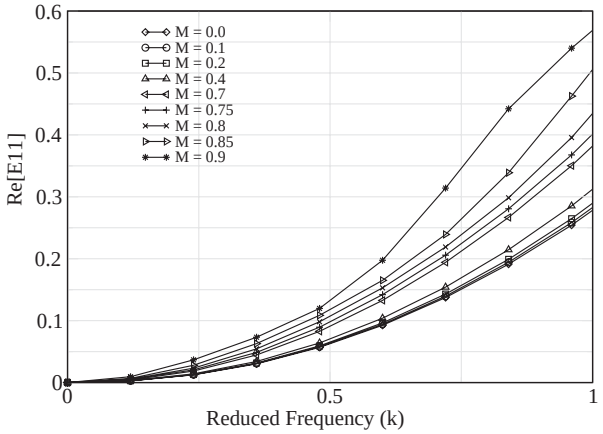

Fig. 1. Mach number influence on E_{11}. Real part.

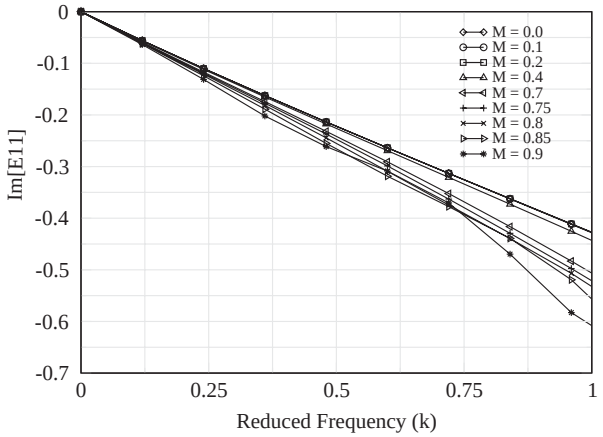

Fig. 2. Mach number influence on E_{11}. Imaginary part.

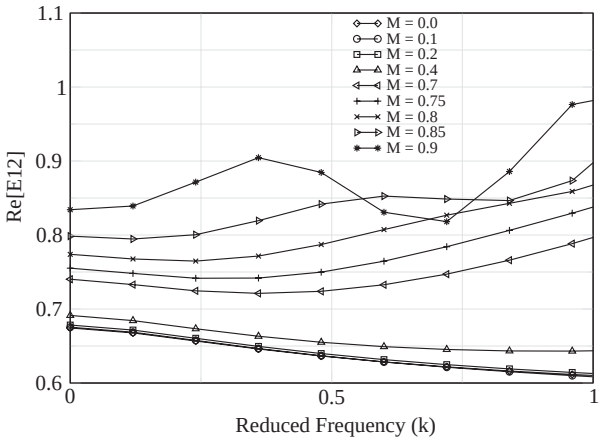

Fig. 3. Mach number influence on E_{12}. Real part.

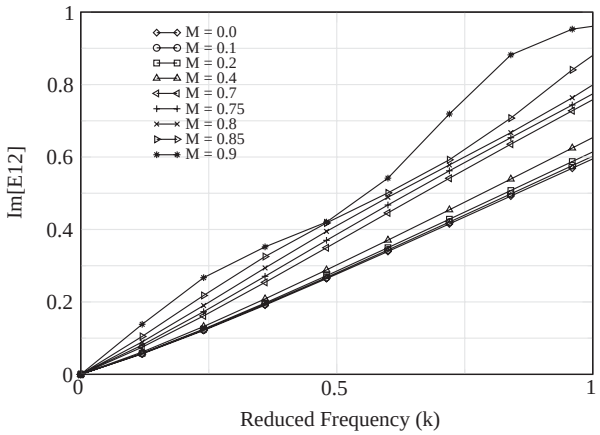

Fig. 4. Mach number influence on E_{12}. Imaginary part.

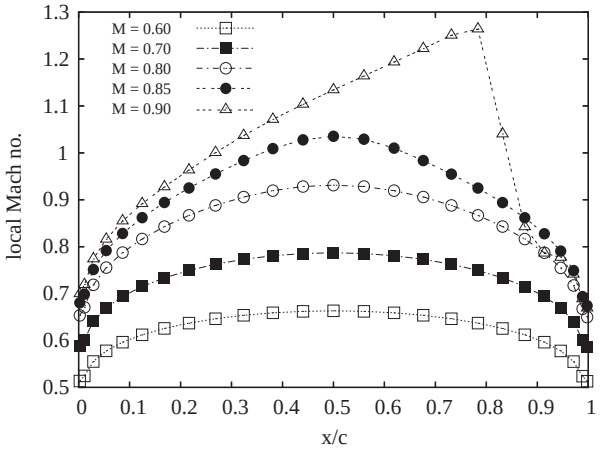

Fig. 5. Local Mach number distribution at the root section of the rectangular wing analyzed in Guruswamy and Goorjian (1982) for five different values of m_B.

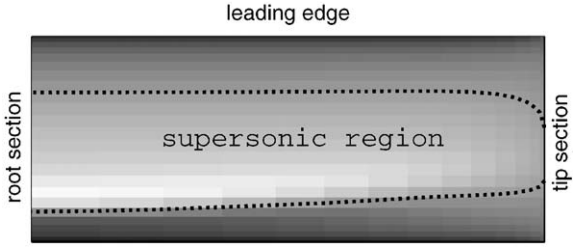

Fig. 6. Local Mach number distribution on the wing surface for $m_B = 0.9$. The dotted line bounds the supersonic region.

calculation presented by Guruswamy and Goorjian (1982). In particular, the error on the flutter speed value predicted by this methodology is less than 3.5% for all the regimes analyzed.

Finally, for μ denoting the wing-to-air-mass density ratio (Guruswamy and Goorjian, 1982), in Fig. 9 the flutter speed parameter v_B/μ is plotted against the Mach number, for $0.7 \leqslant m_B \leqslant 0.92$. Although the shock occurring in the steady-state solution is not particularly strong because of the limited thickness of the section and the zero angle of

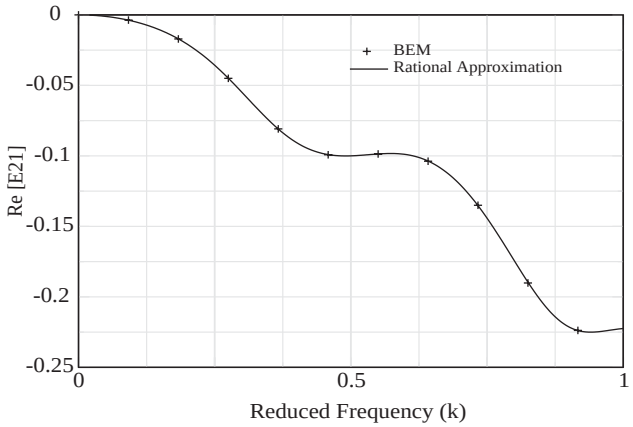

Fig. 7. Approximation of E_{21}. Real part.

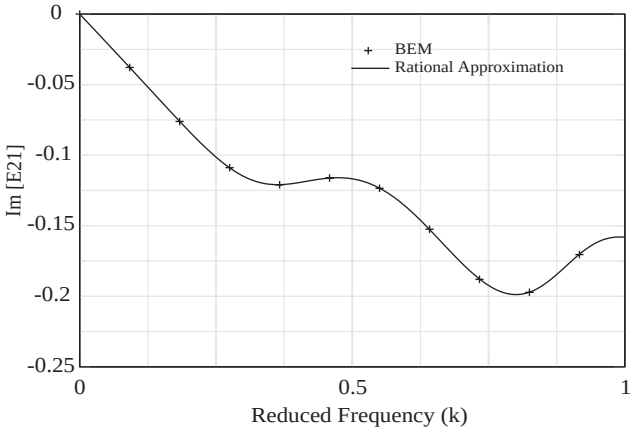

Fig. 8. Approximation of E_{21}. Imaginary part.

Table 1
Nondimensional flutter speed versus Mach number

m_B	$\hat{U}$, experimental (Guruswamy and Goorjian, 1982)	$\hat{U}$, numerical (Guruswamy and Goorjian, 1982)	ROM (present)
0.715	3.83	4.30	3.73
0.851	4.55	5.60	4.61
0.913	4.94	8.80	4.85

Table 2
Reduced flutter frequency versus Mach number

m_B	k, experimental (Guruswamy and Goorjian, 1982)	k, numerical (Guruswamy and Goorjian, 1982)	ROM (present)
0.715	0.232	0.250	0.199
0.851	0.162	0.120	0.133
0.913	0.122	0.045	0.099

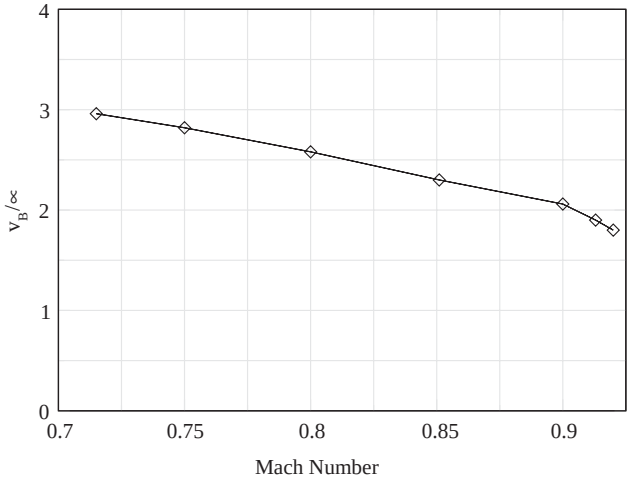

Fig. 9. Flutter speed versus Mach number.

attack in the reference configuration, the well-known *bucketing* effect (i.e., the sudden reduction of the flutter speed in presence of shock waves) is present for $m_B \geqslant 0.9$.

6. Conclusions

A methodology for the identification of an aeroelastic ROM for wings in transonic flows has been presented. It has been obtained through the linearization of a transonic full-potential aerodynamic model, followed by rational approximation of the corresponding aerodynamic transfer functions and coupling with the structural dynamics operator. It has been shown that the wing transonic aeroelasticity problem can be recast in a state–space format and that, therefore, the flutter detection can be achieved through a standard eigenvalue analysis. Numerical results have demonstrated that the effects of flow compressibility at high Mach number have a great influence on the aerodynamic transfer functions, and that the finite-state model used here for their approximation gives highly accurate results. Comparisons with experimental and numerical results available in literature have shown that the aeroelastic ROM presented here yields accurate predictions of flutter boundaries in transonic flow regimes.

Acknowledgment

The authors wish to thank Dr. Gabriele Albanesi for his valuable contribution to the initial phase of the present work.

Appendix A. Matrix $\mathbf{E}^{\chi}$: deformation/potential boundary-condition relation

Let (ξ^1, ξ^2) be a set of curvilinear coordinates defined over the wing surface. Then, in a wing-fixed space the position of a point of the wing is described by

$$\vec{y}(\xi^1, \xi^2, t) = \vec{y}_0(\xi^1, \xi^2) + \vec{d}(\xi^1, \xi^2, t),$$

where $\vec{y}_0$ is the position in the steady-state equilibrium configuration and $\vec{d}$ denotes the perturbation displacement, Eq. (7). From the equation above both the linearized distribution of perturbed outward unit normal vectors (expressed as $\vec{n} = \vec{n}_0 + \vec{n}'$) and the velocity of the wing points (that from elastic deformation added to the translation) may be

derived. These yield the following distribution of linearized perturbation aerodynamic boundary conditions:

$$\chi(\xi^1,\xi^2,t)=\sum_{n=1}^{N_v}\left(\dot{q}_n\,\vec{\psi}_n\cdot\vec{n}_0+q_n\,\vec{v}_B\cdot\vec{n}'_n\right)$$

that, transformed into frequency domain and evaluated at each centroid, gives

$$\tilde{\boldsymbol{\chi}}=\mathbf{E}^{\chi}(s)\,\tilde{\mathbf{q}}. \tag{A.1}$$

In the equation above, $\boldsymbol{\chi}$ and $\mathbf{q}$ are column matrices collecting, respectively, boundary conditions at centroids and wing Lagrangean variables whereas, for $\vec{y}_m=\vec{y}(\xi^1_m,\xi^2_m)$, the entries of the $[M\times N_v]$ matrix $\mathbf{E}^{\chi}$ are given by

$$E^{\chi}_{mn}=s\,\vec{\psi}_n(\xi^1_m,\xi^2_m)\cdot\vec{n}_0(\xi^1_m,\xi^2_m)+\vec{v}_B\cdot\vec{n}'_n(\xi^1_m,\xi^2_m).$$

Appendix B. Matrix $\mathbf{E}^p$: potential/pressure relation

Bernoulli's theorem under small-perturbation assumption yields the potential/wing-surface pressure relationship. For the linearized perturbation pressure, $p'=p-p_\infty$, it yields (with ρ_∞ denoting undisturbed-flow density)

$$\frac{p'}{\rho_\infty}=\frac{v_0^2}{2c_\infty^2}\dot{\varphi}-\left(1+\frac{\vec{v}_B\cdot\vec{v}_0}{c_\infty^2}\right)\left[\dot{\varphi}+(\vec{v}_B-\vec{v}_0)\cdot\nabla\varphi\right]$$

that, transformed into frequency domain, may be recast in the matrix form

$$\tilde{\mathbf{p}}'=\mathbf{E}^p(s)\,\tilde{\boldsymbol{\varphi}}. \tag{B.1}$$

Matrix $\mathbf{E}^p$, of dimensions $[M\times N_t]$, is expressed as

$$\mathbf{E}^p(s)=s\,\mathbf{H}\,\mathbf{T}^B+\mathbf{W}\,\mathbf{G}^B_{gr},$$

where, for δ_{km} denoting the Kronecher delta, the $[M\times M]$ matrix $\mathbf{H}$ and the $[M\times M\times 3]$ matrix $\mathbf{W}$ are, respectively, defined as

$$H_{km}=-\rho_\infty\left(1+\frac{\vec{v}_B\cdot\vec{v}^k_0}{c_\infty^2}-\frac{\vec{v}^k_0\cdot\vec{v}^k_0}{2c_\infty^2}\right)\delta_{km},$$

$$W_{kmj}=\rho_\infty\left(1+\frac{\vec{v}_B\cdot\vec{v}^k_0}{c_\infty^2}\right)(\vec{v}_B-\vec{v}^k_0)\cdot\vec{i}_j\;\delta_{km}.$$

Appendix C. Matrix $\mathbf{E}^f$: pressure/force relation

The generalized aerodynamic forces are obtained by projecting the pressure distribution onto the shape functions describing elastic deformation. Their expression is

$$f_n=-\sum_{m=1}^{M}\int_{\mathsf{S}_m}p'\,\vec{n}\cdot\vec{\Psi}_n\,\mathrm{d}\mathsf{S},$$

or, in frequency-domain matrix form,

$$\tilde{\mathbf{f}}=\mathbf{E}^f\,\tilde{\mathbf{p}}', \tag{C.1}$$

with the $[N_v\times M]$ matrix $\mathbf{E}^f$ defined as

$$E^f_{nm}=-\int_{\mathsf{S}_m}\vec{n}\cdot\vec{\Psi}_n\,\mathrm{d}\mathsf{S}.$$

References

Doggett, R.V., Rainey, A.G., Morgan, H.G., 1959. An experimental investigation of aerodynamic effects of airfoil thickness on transonic flutter characteristics. NASA Technical Memorandum X-79.

Ehlers, S.E., Weatherill, W.H., 1982. A harmonic analysis method for unsteady transonic flow and its application to the flutter of airfoils. NASA Contract Report 82-3537.

Fung, Y.C., 1969. Theory of Aeroelasticity. Dover Publications, New York.

Fung, K.Y., Yu, N.J., Seebass, R., 1978. Small unsteady perturbations in transonic flows. AIAA Journal 16, 815–822.

Gennaretti, M., Mastroddi, F., 2004. Study of reduced-order models for gust-response analysis of flexible wings. Journal of Aircraft 41, 304–313.

Gennaretti, M., Ponzi, C., 1999. Finite-state aerodynamic modelling for gust load alleviation of wing-tail configurations. The Aeronautical Journal 103, 147–158.

Gennaretti, M., Corbelli, A., Mastroddi, F., 2000. A comparison among some aeroelastic models for the stability analysis of a flap-lag-torsion helicopter rotor in hover. 26th European Rotorcraft Forum, The Hague, The Netherlands.

Ghiringhelli, G.L., Mantegazza, P., 1993. Interpolation extrapolation and modeling of unsteady linear(ized) aerodynamic forces. International Forum on Aeroelasticity and Structural Dynamics, Strasbourg, France.

Guruswamy, G.P., Goorjian, P.M., 1982. Comparison between computations and experimental data in unsteady three-dimensional transonic aerodynamics, including aeroelastic applications. NASA Technical Note 82-06090.

Iemma, U., Morino, L., 1997. Steady two-dimensional analysis using a boundary integral equation method. Journal of Fluids and Structures 11, 247–269.

Jameson, A., 1975. Transonic potential flow calculation using conservation form. AIAA Second Computational Fluid Dynamics Proceedings, Hartford, Connecticut, USA, pp. 148–161.

Lucia, D.J., Beran, P.S., Silva, W.A., 2004. Reduced-order modeling: new approaches for computational physics. Progress in Aerospace Sciences 40, 51–117.

Morino, L., Iemma, U., 1993. Boundary integral equations and conservative dissipation schemes for full-potential transonic flow. Computational Mechanics 13, 90–100.

Silva, W.A., Bartels, R.E., 2004. Development of reduced-order models for aeroelastic analysis and flutter prediction using the CFL3Dv6.0 code. Journal of Fluids and Structures 19, 729–745.

Williams, M.H., 1979. The linearization of transonic flows containing shocks. AIAA Journal 17, 394–397.